Imaging Single Quantum Dots in Three-Dimensional Photonic Crystals

Michael Barth,* Roman Schuster,† Achim Gruber,‡ and Frank Cichos

Photonics and Optical Materials, Institute of Physics, Chemnitz University of Technology, 09107 Chemnitz, Germany

(Received 10 February 2006; published 21 June 2006)

Performing fluorescence wide-field microscopy we have imaged single semiconductor quantum dots deep inside a 3-dimensional photonic crystal prepared from colloidal polymer beads. Exploring the emission diffraction patterns in defocused images of quantum dots we demonstrate that the direction-dependent photonic stop band imprints an anisotropy to the angular emission of a single quantum dot. Hence a single, quasi-point-like emitter is manipulated to radiate its photons only to certain well-defined directions by means of the anisotropic light propagation in photonic crystals. The experiments thus provide new routes to evaluate local, frequency selective optical properties in 3-dimensional photonic crystals employing single emitters.

DOI: 10.1103/PhysRevLett.96.243902 PACS numbers: 42.70.Qs, 78.67.Hc

Manipulating light is at the heart of photonics research with ultimate goals like control over the emission of a single chromophore and thus over many applications in quantum information processing [1], light emitting devices [2], or solar cells [3]. Such emission control requires suitable dielectric materials, which influence light propagation on a microscopic level. Photonic crystals—a new class of materials with periodic dielectric structure—offer such properties [4,5]. They redistribute the photon density of states, expelling even vacuum fluctuations of the electromagnetic field from certain spectral regions. As a consequence light may become localized [6,7], spontaneous emission is modified [5,8,9], and propagation may become strongly directive [10–14]. The fundamental difficulty in all experiments investigating the electromagnetic mode structure of 3-dimensional photonic crystals is related to the spatial dependence of the optical properties. Because of the spatial variation of the refractive index in a photonic crystal, the optical density of states depends on position and therefore a variety of effects, such as enhancement or inhibition of spontaneous emission [8], depend on the position of the emitter inside the material. This local electromagnetic mode structure, which has so far not been investigated in 3-dimensional crystals due to lack of a suitable experimental technique, may become accessible employing single emitters.

Here we show for the first time that the local optical properties of photonic crystals can be revealed with the help of single emitters embedded deep inside a 3-dimensional photonic crystal. We demonstrate that the photonic stop band of artificial colloidal opals modifies the emission anisotropy of single CdSe/ZnS core-shell quantum dots. The imprinted anisotropy can be detected by defocused wide-field imaging of single quantum dots. Our experimental results thus open the way to explore the true local density of states in photonic crystals, and provide a basis for efficient use of the local optical properties of photonic crystals in applications.

Colloidal photonic crystals have been prepared by vertical deposition of polystyrene beads (260 nm diameter, 1 wt %, Duke Scientific) on quartz cover slides (200 μm thickness). The resulting photonic crystal was characterized by transmission and reflection measurements with a Shimazu uv-visible photospectrometer [see Fig. 1(d) for the reflection spectrum at normal incidence]. The photonic crystal was subsequently doped with a $10^{-8}M$ solution of water soluble CdSe/ZnS core-shell quantum dots (Evident Technologies, Fort Orange, 600 nm mean emission wavelength), which distributes the quantum dots randomly over the photonic crystal. CdSe/ZnS core-shell quantum dots were selected as emitters, since they provide bright, photostable emission with a narrow linewidth ($\approx$15 nm FWHM and therefore narrower than the photonic stop band width $\approx$ 40 nm) at room temperature and a size dependent emission wavelength [15]. Thus spectrally selective probing of the photonic stop band with single quantum dots of different size is feasible [see Fig. 1(e)].

Single quantum dots were imaged in a home-built fluorescence wide-field microscope equipped with a 100 $\times$, 1.35 NA microscope objective (Olympus), an intensified CCD (Roper Scientific Cascade:512B) and a diode-pumped solid state laser (532 nm, 0.5 mW excitation power). Fluorescence images (500 frames, 300 pixels $\times$ 300 pixels) were recorded at each focal position at a frame rate of 2 Hz with an exposure time of 500 ms and an excitation power of 0.5 mW in front of the microscope objective. The focus position was varied with the help of a piezo stage (PI), starting at the substrate–photonic-crystal interface and stepping through the crystal with a step size of 500 nm. Structural imperfections allow locating the substrate–photonic-crystal interface with an accuracy of $\pm$150 nm. Figures 1(a)–1(c) show sum images of all recorded frames for different sample areas and focal depths d. Most of the quantum dots in each of the three images are out of focus due to the random distribution of emitters in the photonic crystal, which results in a characteristic diffraction pattern encircling each quantum dot image.

Figure 1(f) shows two selected quantum dots at different distances from the photonic-crystal–quartz interface (d = 0 μm and $d = 3.7$ μm) as determined from images at

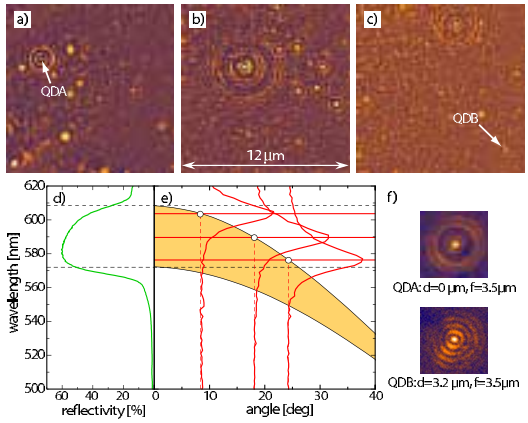

FIG. 1 (color online). Fluorescence images of single CdSe/ZnS quantum dots embedded in a colloidal photonic crystal detected at different focus positions d relative to the photonic-crystal–quartz interface: (a) $d = 2.5\ \mu$m, (b) $d = 4.98\ \mu$m, (c) $d = 6.8\ \mu$m inside the opal. (d) Experimental reflection spectrum along the [111] direction of the prepared photonic crystal showing a photonic stop band in the range of 570 to 610 nm. The horizontal dashed lines denote the range of the photonic stop band. (e) Shift of the photonic stop band with increasing angle to the [111] direction together with emission spectra of three different single CdSe/ZnS quantum dots [light gray curves (red online)]. The solid horizontal lines mark the center emission wavelength of the quantum dots. The vertical dashed lines show the corresponding aperture angles of the Bragg cones expected for the emission wavelength. (f) Fluorescence image of two selected quantum dots located at the photonic-crystal–quartz interface [top, $d = 0\ \mu$m marked QDA in (a)] and $d = 3.7\ \mu$m [bottom, marked QDB in (c)] inside the photonic crystal. Both quantum dots are by $f = 3.5\ \mu$m out of focus.

different focal depth d. Both quantum dots are out of focus by $f = 3.5\ \mu$m. Because of the emission intermittence of the quantum dots [16,17] the images were obtained by summing up only those frames in which the particular quantum dot is emitting. Comparing the two spots in Fig. 1(f) suggests that the different patterns arise from the photonic stop band of the opal. The characteristic pattern, which emerges from diffraction of the emitted light into the aperture of the microscope objective should therefore carry information on the emission anisotropy of the chromophore and information on any modification of the optical mode density at the position of the emitter. Image analysis with respect to the first issue has been employed in the literature to yield information on the orientation and shape of the transition moment of single emitters [18–20]. The second issue, which we address here for the first time, becomes important if an emitter is placed inside a material in which propagation of light is anisotropic. This is particularly the case for a photonic crystal with its direction-dependent photonic stop band, which imprints an additional anisotropy on the light emission [11] if the emission wavelength coincides with the spectral region of the photonic stop band. In the simplest case, the introduced anisotropy for a quantum dot with a certain emission wavelength can be described by a cone—referred to as the Bragg cone—with an half-aperture α, in which the light propagation within the crystal is prohibited [see Figs. 1(e) and 3(a)]. The aperture angle of the Bragg cone is related to the shift of the stop band with increasing angle to the [111] direction. Figure 1(e) shows this relation [11]. Angle α goes to zero at a wavelength of about 610 nm and is largest at about 570 nm. Below 570 nm the cone will reduce to a cone shell. Note that this anisotropy is not necessarily related to any loss but to a spatial redistribution of photons and thus is in principle equivalent to modifications of the angular emission characteristics of a single emitter.

To substantiate the effect of the photonic stop band on the diffraction pattern we first analyze the quantum dot located at the photonic-crystal–quartz interface (QDA), at various defocusing depths ($f = 1.6\ \mu$m to $f = 4.4\ \mu$m) and compare the patterns obtained to theoretical calculations. This comparison serves as a quantitative reference for the quality of the images and the accuracy of the employed model. Our theoretical description is based on numerical calculations adapting the model by Böhmer *et al.* [21] to the present experimental conditions. This includes a 2-dimensional transition moment for the CdSe quantum dots [22,23] and a dielectric interface between the immersion oil ($n_{\text{oil}} = 1.51$) and the quartz cover slide ($n_{\text{quartz}} = 1.458$). The interface between the quartz slide and the photonic crystal has not been treated explicitly since the photonic crystal has an effective refractive index of $\bar{n}_{PC} = 1.46$ and is therefore almost perfectly index matched to the quartz. The obtained experimental and theoretical emission patterns are presented in Fig. 2 (top and middle row) and are in excellent agreement. All patterns are perfectly circular even though the 2-dimensional transition dipole of the CdSe quantum dots suggests an angular anisotropy [20,22,24]. The reason for this is the large distance of the emitter from the quartz–immersion-oil interface ($\approx 200\ \mu$m), which leads to a strong blurring of all asymmetric features in the imaging pattern. The angular symmetry of the images allows calculation of an angle integrated radial intensity distribution, which is depicted in Fig. 2 (bottom row) for all focal positions comparing the experimental [light gray curve (red online)] and theoretical data [dark gray curve (blue online)]. The graphs demonstrate that the coincidence between experiment and theory goes far beyond a simple qualitative agreement but shows a remarkably good quantitative agreement for nearly all focal positions. While the patterns at small defocusing $f < 2.5\ \mu$m exhibit a decaying intensity of the rings from the inside to the outside, all patterns at focal positions $f > 3\ \mu$m show a characteristic sequence of bright and dim rings. This sequence of bright and dim diffraction rings expected at $f = 3.5\ \mu$m defocusing is missing in the emission pattern of QDB. This difference cannot be explained just by a different emission wavelength or distance

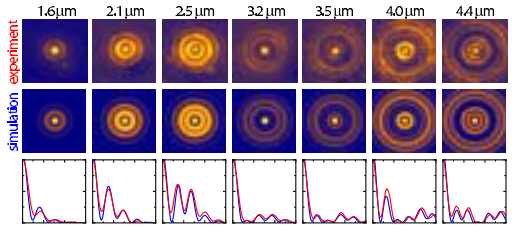

FIG. 2 (color online). Top row: Fluorescence images of a single CdSe/ZnS quantum dot (QDA) located at the photonic-crystal–quartz interface. The images are taken at different focus positions relative to the location of the quantum dot ($d = 0$ μm, $f = 1.6$ μm and $f = 4.4$ μm defocusing). Middle row: Calculated defocused wide-field images of a single quantum dot at the experimentally adjusted focus positions. Bottom row: Comparison of the radial intensity distribution of the experimental [light curve (red online)] and theoretical image [dark curve (blue online)].

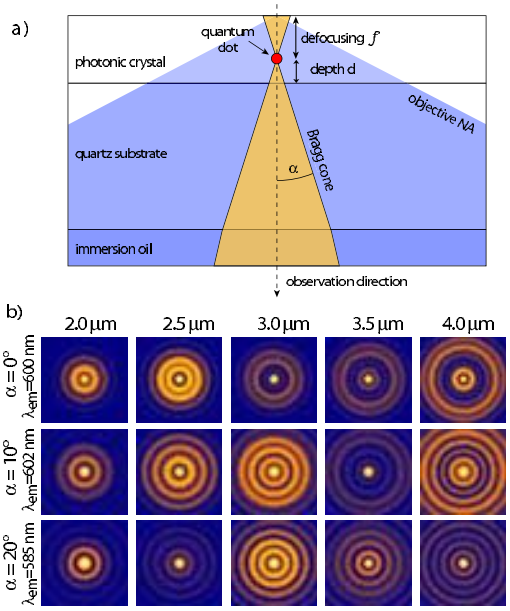

FIG. 3 (color online). (a) Sketch of the experimental idea. If the quantum dot emission is within the photonic stop band of the opal, light propagation is prohibited within a certain cone (Bragg cone) with an aperture angle α. Light which would propagate within this cone is not able to contribute to the image formation by the microscope objective (with a collecting numerical aperture NA) and therefore distorts the image especially at slight defocusing f. (b) Calculated defocusing series for a single quantum dot in a photonic crystal at various aperture angles α of the Bragg cone. The numbers above the top row denote the position of the focus f relative to the quantum dot location. The corresponding aperture angle and the emission wavelength of the quantum dot are denoted on the side of each row.

from the refracting quartz–immersion-oil interface, which suggests a strong influence of the photonic stop band on the angular distribution of the emitted light and is supported by the fact that at a depth of $d = 3.7$ μm ($\approx$25 lattice planes) Bragg reflections are already well developed.

To obtain a quantitative picture of these modifications, we have incorporated the simplest model of a Bragg cone into the described model calculations, by defining an angular range in which propagation is suppressed [see Fig. 3(a)]. The half-aperture angle of the Bragg cone is selected according to the emission wavelength of the quantum dot [Fig. 1(e)]. Although this model is a very rough assumption neglecting all other effects of the photonic band structure [11,13,14], it enables us to demonstrate the basic effects on the emission patterns. The results of this calculation are shown in Fig. 3(b) for two different half-aperture angles in comparison with the undisturbed emission patterns for an emission wavelength of 600 nm. We find that a Bragg cone of only 10° half-aperture angle (about 1/6 of the objective lens half collection angle), corresponding to an emission wavelength of 600 nm, should already induce visible deviations from an undisturbed diffraction pattern. For a half-aperture angle of 20° (580 nm), the effect of the Bragg cone becomes very strong, especially at higher defocusing ($f > 2.5$ μm). Here the sequence of bright and dim rings as depicted in Fig. 2 is altered to a simple decaying ring intensity as observed experimentally for the quantum dot depicted in Fig. 1(f).

Based on these calculations we have carried out an analysis of the emission patterns of several quantum dots located deep inside the photonic crystal. We have fitted the experimentally obtained diffraction patterns at various focal positions, using aperture angles of the Bragg cone corresponding to the wavelength of emission. We would like to emphasize that one pair of parameters (angle α and emission wavelength) has to match a whole series of emission patterns at different defocusing values f, where the calculated defocusing distance further has to fit the adjusted defocusing of the setup. Figures 4(a) and 4(b) show the experimental images of the two different quantum dots together with the radial intensity distributions (experiment, red; simulation, blue).

The characteristic dim and bright diffraction rings are missing in both defocusing series especially at the larger focus positions ($f > 3$ μm), which agrees qualitatively with the model calculation shown in Fig. 3(b). The quantum dot shown in Fig. 4(a) corresponds to a half-aperture angle of the Bragg cone of 19° (588 nm). The second quantum dot shown in Figure 4(b) is emitting at 595 nm and exhibits a half-aperture angle of the Bragg cone of about 15°. The radial intensity distributions of all emission patterns are shown below the experimental images and reveal a very good quantitative agreement of experiment and simulation. Thus our experiments show for the first time that anisotropic propagation within a photonic crystal can be monitored by examination of the emission of a single emitter. Combined with a more precise knowledge of the position of the quantum dot within the unit cell and the 3-dimensional structure of the particular photonic crystal based, e.g., on tomographic methods [25], the method

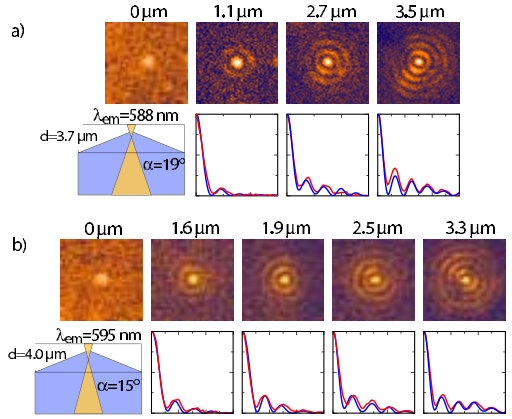

FIG. 4 (color online). a) Experimental defocusing series for a single CdSe/ZnS quantum dot embedded in a colloidal photonic crystal. The quantum dot is $d = 3.7$ μm away from the photonic-crystal–quartz interface and obeys a Bragg cone aperture angle of 19° at an emission wavelength of 588 nm. b) Experimental defocusing series for a single CdSe/ZnS quantum dot embedded in a colloidal photonic crystal. The quantum dot is $d = 4.0$ μm away from the photonic-crystal–quartz interface and obeys a Bragg cone aperture angle of 15° at an emission wavelength of 595 nm. The graphs below the images in (a) and (b) show the radial intensity distributions of the experimental images [light curve (red online)] compared to the calculated ones [dark curve (blue online)].

employed allows a true local investigation of the interaction of a quasi-point-like emitter with the mode structure of the 3-dimensional photonic crystal. While the rough approximation of the photonic stop band effect introduced into the model calculations describes the observations well, effects like finite homogeneous linewidth and enhanced emission in certain directions of the photonic crystal will be taken into account in future calculations. The refinement of the model and the extension of the measurements to, e.g., quantum dots emitting at the short wavelength stop band edge or even to stronger photonic crystals, will give a wealth of new information on the spatial and spectral dependence of light propagation inside 3-dimensional photonic crystals.

The results of our study imply that the manipulation of light emitted by even a single emitter can be detected within complex photonic systems. This is a starting point for the manipulation of the radiative properties of single photon sources in 3-dimensional photonic crystals. We have demonstrated that single quantum dots inside a weak photonic system do not emit light as predicted by their transition moment but with an extra angular anisotropy introduced by the stop band of the photonic crystal. This effect together with spectrally selective highly directive light propagation as demonstrated in various studies [11,13] provides the means of preparing, e.g., single photon sources with highly directional emission. We expect that our results will be of use for fundamental local investigations of the optical properties of 3-dimensional photonic crystals.

*Present address: Nano-Optics, Institute of Physics, Humboldt University Berlin, Hausvogteiplatz 5-7, 10117 Berlin, Germany.
†Present address: Leibniz Institute for Solid State and Materials Research, Helmholtzstraße 20, 01069 Dresden, Germany.
‡Present address: PicoQuant GmbH, Rudower Chaussee 29, 12489 Berlin, Germany.

[1] N. Vats and T. Rudolph, J. Mod. Opt. **48**, 1495 (2001).
[2] L. Chen and A. V. Nurmikko, Appl. Phys. Lett. **85**, 3663 (2004).
[3] S. Nishimura, N. Abrams, B. A. Lewis, L. I. Halaoui, T. E. Mallouk, K. D. Benkstein, J. van de Lagemaat, and A. J. Frank, J. Am. Chem. Soc. **125**, 6306 (2003).
[4] S. John, Phys. Rev. Lett. **58**, 2486 (1987).
[5] E. Yablonovitch, Phys. Rev. Lett. **58**, 2059 (1987).
[6] S. John, Phys. Today **44**, No. 5, 32 (1991).
[7] H. Gersen, T. J. Karle, R. J. P. Engelen, W. Bogaerts, J. P. Korterik, N. F. van Hulst, T. F. Krauss, and L. Kuipers, Phys. Rev. Lett. **94**, 073903 (2005).
[8] P. Lodahl, A. F. van Driel, I. S. Nikolaev, A. Irman, K. Overaa, D. Vanmaekelbergh, and W. L. Vos, Nature (London) **430**, 654 (2004).
[9] M. Fujita, S. Takahashi, Y. Tanaka, T. Asano, and S. Noda, Science **308**, 1296 (2005).
[10] P. Kramper, M. Agio, C. M. Soukoulis, A. Birner, F. Müller, R. Wehrspohn, U. Goesele, and V. Sandoghdar, Phys. Rev. Lett. **92**, 113903 (2004).
[11] M. Barth, A. Gruber, and F. Cichos, Phys. Rev. B **72**, 085129 (2005).
[12] A. F. Koenderink and W. L. Vos, Phys. Rev. Lett. **91**, 213902 (2003).
[13] L. Bechger, P. Lodahl, and W. Vos, J. Phys. Chem. B **109**, 9980 (2005).
[14] J. Mizuguchi, S. T. Y. Tanaka, and M. Notomi, Phys. Rev. B **67**, 075109 (2003).
[15] S. V. Gaponenko, *Optical Properties of Semiconductor Nanocrystals* (Cambridge University Press, Cambridge, 1998).
[16] M. Nirmal, B. O. Dabbousi, M. G. Bawendi, J. J. Macklin, J. K. Trautman, T. D. Harris, and L. E. Brus, Nature (London) **383**, 802 (1996).
[17] A. Issac, C. von Borczyskowski, and F. Cichos, Phys. Rev. B **71**, 161302 (2005).
[18] J. Sepiol, J. Jasny, J. Keller, and U. P. Wild, Chem. Phys. Lett. **273**, 444 (1997).
[19] A. P. Bartko and R. M. Dickons, J. Phys. Chem. B **103**, 11 237 (1999).
[20] R. Schuster, M. Barth, A. Gruber, and F. Cichos, Chem. Phys. Lett. **413**, 280 (2005).
[21] M. Böhmer and J. Enderlein, J. Opt. Soc. Am. B **20**, 554 (2003).
[22] Recent studies indicate that CdSe quantum dots rather possess a 3-dimensional transition moment (2D + 1D) at room temperature due to a splitting of the valence band. See Refs. [20,24].
[23] I. Chung, K. T. Shimizu, and M. G. Bawendi, Proc. Natl. Acad. Sci. U.S.A. **100**, 405 (2003).
[24] D. Patra, I. Gregor, J. Enderlein, and M. Sauer, Appl. Phys. Lett. **87**, 101103 (2005).
[25] R. Magerle, Phys. Rev. Lett. **85**, 2749 (2000).